KLOE Note 173
June 2002

Fit to the invariant mass spectra of the decays $\phi \to \pi^0\pi^0\gamma$ and $\phi \to \eta\pi^0\gamma$

C.Bini[a], P.Gauzzi[a], S.Giovanella[b], D.Leone[a], S.Miscetti[b]

[a] *Università "La Sapienza" and INFN Roma*
[b] *Laboratori Nazionali di Frascati dell'INFN*

Abstract

In this paper we report the theoretical framework used to describe the decays $\phi \to \pi^0\pi^0\gamma$ and $\phi \to \eta\pi^0\gamma$ and the procedure developed to fit the pseudoscalars invariant mass spectra. These processes are determined to be dominated by the intermediate state $f_0\gamma$ and $a_0\gamma$ respectively. A sizeable contribution ($\sim 20\%$) due to $\sigma\gamma$ is also observed in the $\phi \to \pi^0\pi^0\gamma$ channel.

1 Introduction

The ϕ radiative decays into $\pi^0\pi^0\gamma$ and $\eta\pi^0\gamma$ are dominated by the decays $\phi \to f_0\gamma$ and $\phi \to a_0\gamma$. The rate of these two decays, and the shape of the invariant mass spectra, are important in clarifying the controversial nature of the scalar particles $f_0(980)$ and $a_0(980)$ which are, respectively, the isospin singlet and the neutral element of the isospin triplet of the lowest mass scalar mesons (S in the following). Furthermore, the ratio of the two rates is sensible to possible strong isospin mixing between the isospin singlet and the neutral element of the isospin triplet.

These decays have been widely studied in the first period of KLOE data taking, looking at five photons final states (for $\pi^0\pi^0\gamma$ and $\eta\pi^0\gamma$ with $\eta \to \gamma\gamma$) and at 2 tracks + 5 photons final state (for $\eta\pi^0\gamma$ with $\eta \to \pi^+\pi^-\pi^0$) [1, 2, 3]. For these three channels, the distribution of the invariant mass, m, of the two pseudoscalar particles ($m = M_{\pi\pi},\ M_{\eta\pi}$) has been obtained. In order to extract the contribution due to the intermediate states $\phi \to S\gamma$, S being either f_0 or a_0, the mass spectra have been fitted using a general theoretical framework mainly due to N.N.Achasov and co-workers [4, 5, 6]. In this context, we have also included the expected contribution due to $\phi \to \rho^0\pi^0$ with $\rho^0 \to \pi^0\gamma$ or $\rho^0 \to \eta\gamma$ (the so called vector meson dominance, VMD, term [7]). For the $\pi^0\pi^0\gamma$ final state, the possibility of $\phi \to \sigma\gamma$ has also been considered.

In this memo we describe the theoretical framework, the fit procedures and we present and discuss the fit results.

2 Theoretical framework

The decay $\phi \to ab\gamma$, with ab a pair of pseudoscalar mesons of invariant mass m, can be expressed in the following way:

$$\frac{d\Gamma(\phi \to ab\gamma)}{dm} = \frac{d\Gamma_S}{dm} + \frac{d\Gamma_{\mathrm{VMD}}}{dm} + \frac{d\Gamma_{\mathrm{int}}}{dm}\cos\phi_{SV} \tag{1}$$

where the first intermediate term corresponds to a radiative transition to a scalar particle ($S\gamma$), the second one refers to possible vector contributions ($\rho\pi$) while the third one represents the interference between the two previous terms with ϕ_{SV} being a free interference phase. In this section, the most relevant parts of the used theoretical framework are summarized to introduce the reader to the terminology used in the fit section. We use here and in the following either $d\Gamma/dm$ or $d\mathrm{BR}/dm$, (BR is the branching ratio of the considered channel), simply related by $d\mathrm{BR}/dm = (1/\Gamma_\phi)d\Gamma/dm$.

2.1 Scalar production contribution

The differential width $d\Gamma_S/dm$ of the decay $\phi \to ab\gamma$, proceeding via an intermediate scalar particle decaying to ab, is expressed in the following way [4]:

$$\frac{d\Gamma(\phi \to S\gamma \to ab\gamma)}{dm} = \frac{2m^2}{\pi}\frac{\Gamma(\phi \to S\gamma)\Gamma(S \to ab)}{|D_S|^2} \tag{2}$$

We describe here each term of this equation according to $\phi S\gamma$ coupling via kaon loop and to $\phi\sigma\gamma$ point-like coupling.

2.1.1 The $\phi S\gamma$ coupling via charged kaon loop

The formulation used in the following assumes that the $S\gamma$ term proceeds through charged kaon loops as schematically shown in Fig. 1(a). The couplings between the virtual kaons and the ϕ or S are pointlike (i.e. the possibility of extended $K\overline{K}$ moleculas is not considered). The width of the radiative transition is described trough a K^+K^- loop as follows:

$$\Gamma(\phi \to S\gamma, m) = \frac{1}{3} \cdot \frac{|g_{\mathrm{kl}}(m)|^2}{4\pi M_\phi^2} \cdot \left(\frac{M_\phi^2 - m^2}{2M_\phi}\right) \tag{3}$$

where m is the mass of the scalar given by the invariant mass of the ab system, $g_{\mathrm{kl}}(m) = g_{\phi K\overline{K}} \cdot g_{SK\overline{K}} \cdot g(m)$ is the kaon loop term given by the two coupling constants of the ϕ and the scalar S to the kaon loop $g_{\phi K\overline{K}}$ and $g_{SK\overline{K}}$ respectively, times a function $g(m)$. The term in parenthesys is the photon energy E_γ [1], due to the phase-space. The value of $g_{\phi K\overline{K}}$ is a well known number, related to the visible width of $\phi \to K^+K^-$ [2], while the coupling between the scalar S and the K^+K^- is a parameter to be determined. The function $g(m)$ describes the kaon loop amplitude and it is explicitely written in Ref. [4], although the same result, with different notations, can be found also in Ref. [8]. This function satisfies the gauge invariance condition and is proportional to E_γ at low photons energy while acting as a form factor at higher E_γ values. To show the threshold behaviour hidden in $g(m)$ we have reported in Fig. 2 the distribution of $|\Re e(g(m))|^2$ and $|\Im m(g(m))|^2$.

The width of S going to the final state ab is given by:

$$\Gamma(S \to ab) = \frac{g_{Sab}^2}{16\pi m} \sqrt{\left(1 - \frac{m_+^2}{m^2}\right)\left(1 - \frac{m_-^2}{m^2}\right)} \tag{4}$$

where $m_\pm = m_a \pm m_b$, with $m_{a,b}$ being the masses of the pseudoscalar mesons. For the $\eta\pi^0$ case, the coupling constant used is $g_{a_0\eta\pi}$ while for the $\pi^0\pi^0$ case is $g_{f_0\pi^+\pi^-}$. In the latter case the observed width, $\Gamma(f_0 \to \pi^0\pi^0)$, is equivalent to $0.5 \cdot \Gamma(f_0 \to \pi^+\pi^-)$.

For the inverse propagator of the scalar meson, D_S, the correct formula, which takes into account the finite-width corrections and the behaviour due to the proximity of the $K\overline{K}$ thresholds [4] is:

$$D_S(m) = m_S^2 - m^2 + \Re e(\Pi_S(m_S)) - \Pi_S(m) \tag{5}$$

[1] In the c.m.s the relation between the photon energy, the ϕ mass and m is $E_\gamma = (M_\phi^2 - m^2)/(2 \cdot M_\phi)$. The differential width in m or E_γ are related by $d\Gamma/dm = d\Gamma/dE_\gamma \cdot (m/M_\phi)$.

[2] The relation is $\Gamma = g_{\phi K\overline{K}}^2 M_\phi \cdot (1 - 4M_K^2/M_\phi^2)/(48\pi)$. The constant $g_{\phi K\overline{K}}$ is adimensional and, inserting the PDG-2001 values, we get $g_{\phi K\overline{K}} = 4.59$.

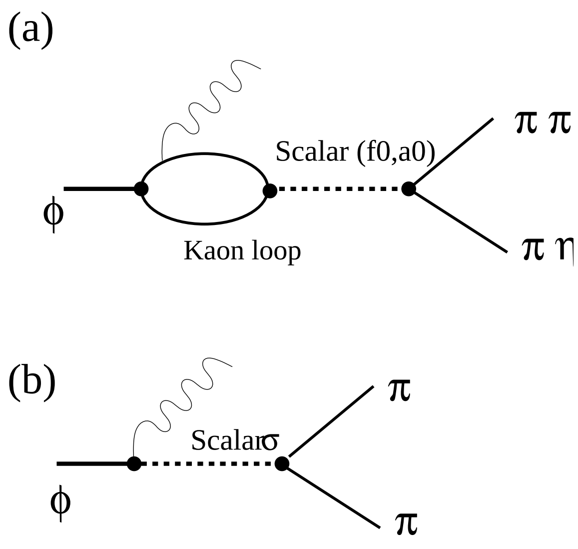

Figure 1: Feynman diagrams describing the $\phi S\gamma$ coupling through a $K\overline{K}$ loop (a) and through direct point-like coupling (b).

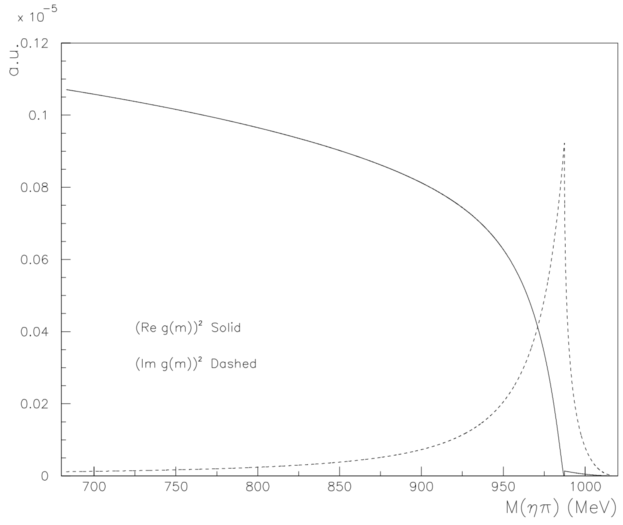

Figure 2: Square of the real and imaginary part of the adimensional function $g(m)$ described in the text.

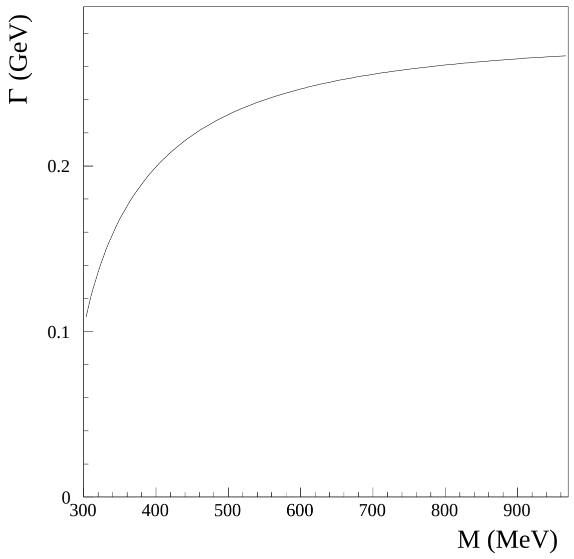

Figure 3: Total width Γ_{f_0} as a function of m.

with m_S the mass of the scalar particle and $\Pi_S(m) = \sum_{ij} \Pi_S^{ij}(m)$ representing the total width of the meson S obtained summing over all the possible final states ij. For the $\pi^0\pi^0\gamma$ case we consider the final states $\pi^+\pi^-$, $\pi^0\pi^0$, $\eta\eta$, K^+K^- and K^0K^0. Following isospin simmetry the total width can be written as:

$$\Pi_{f_0}(m) = 1.5 \cdot \Pi_{f_0}^{\pi^+\pi^-} + \Pi_{f_0}^{K^+K^-} + \Pi_{f_0}^{K^0\overline{K^0}} + \Pi_{f_0}^{\eta\eta} \tag{6}$$

The contribution of $\Pi^{\eta\eta}$ is small but not unrelevant; moreover $g_{f_0K^+K^-} = g_{f_0K^0\overline{K^0}} = g_{f_0K\overline{K}}$ and the relation $g_{f_0\eta\eta} = 0.85 \cdot g_{f_0K\overline{K}}$ from $q\overline{q}q\overline{q}$ model is used. Similarly for the $\eta\pi$ case

$$\Pi_{a_0}(m) = \Pi_{a_0}^{\eta\pi} + \Pi_{a_0}^{K^+K^-} + \Pi_{a_0}^{K^0\overline{K^0}} + \Pi_{a_0}^{\eta'\pi} \tag{7}$$

with $g_{a_0K^+K^-} = g_{a_0K^0\overline{K^0}} = g_{a_0K\overline{K}}$ and $g_{a_0\eta'\pi} = -1.13 \cdot g_{a_0K\overline{K}}$.

The total width of the S meson is a function depending on m (see Fig. 3 for the case $S = f_0$) having a value at the resonance peak of: $-\Im m(\Pi_S(m_S)/m_S)$.

2.1.2 The $\phi\sigma\gamma$ point-like coupling

For the $\phi \to \pi^0\pi^0\gamma$ case only, we have also considered the possibility of a scalar contribution due to the σ meson (a controversial isospin singlet scalar meson) with a point-like $\phi\sigma\gamma$

coupling (see Fig.1 (b))[9]. Actually, there have been recent precise and direct experimental evidence of this meson. The E791 collaboration observed [10] a clear peak at $M_\sigma = 478^{+29}_{-29}$ MeV, with $\Gamma_\sigma = 324^{+47}_{-45}$ MeV in the decay $D^+ \to \sigma\pi^+ \to \pi^+\pi^-\pi^+$. Close mass values, although with larger width, have been also reported in Ref. [11] from CLEO[3]. The $\Gamma_{\phi S\gamma}$ can be written as:

$$\Gamma(\phi \to \sigma\gamma) = \frac{1}{3}\,\frac{|g_{\rm pl}(m)|^2}{4\,\pi M_\phi}\,(\frac{M_\phi^2 - m^2}{2M_\phi}) \tag{8}$$

where $g_{\rm pl}(m) = e \cdot g_{\phi S\gamma} \cdot (\frac{M_\phi^2 - m^2}{2M_\phi})$ and $g_{\phi\sigma\gamma}$, represents the $\phi - \sigma\gamma$ coupling constant. The inverse propagator D_S can be replaced here with a simple relativistic Breit Wigner such as:

$$BW_\sigma = M_\sigma^2 - m^2 - i \cdot M_\sigma \Gamma_\sigma \tag{9}$$

If we use the same formula for $\Gamma(f_0 \to ab)$ and $\Gamma(\sigma \to ab)$, the coupling constant $g_{\phi\sigma\gamma}$ incorporates also the difference between these two mesons in the coupling strengths to the final state. To take into account the interference between $f_0\gamma$ and $\sigma\gamma$ (and similarly the $S\gamma$-VMD interference) the propagator in Eq. (2) has to be replaced with:

$$\frac{1}{D_{f_0+\sigma}} = \frac{1}{D_{f_0}} + \frac{i\, g_{\rm pl}(m)}{g_{\rm kl}(m) \times BW_\sigma} \tag{10}$$

2.2 VMD contribution

The VMD contribution is dominated by $\phi \to \rho^0\pi^0$ followed by the radiative decay $\rho^0 \to P\gamma$ (P being a pseudoscalar meson either η or π^0). Due to the combined effect of the large width of the ρ^0 meson and of the thresholds in the $\rho^0 \to P\gamma$, the amount of these decays cannot be simply evaluated by multiplying the known branching ratios. Several evaluations can be found in the literature [6, 7, 12] giving significantly different expected values. In this paper we use the parametrization given by [6] where the mass spectrum for the background processes is expressed as:

$$\frac{d\Gamma_{\rho\pi}(m)}{dm} = k\frac{(m_\phi^2 - m^2) \cdot p_{ab}}{128\,\pi^3\, m_\phi^3} \int_{-1}^{+1} dx A_{\rho\pi}(m,x) \tag{11}$$

where p_{ab} is given by:

[3]CLEO reports a M_σ of 555 MeV and a Γ_σ of 540 MeV.

$$p_{ab} = \frac{\sqrt{(m^2 - m_-^2)(m^2 - m_+^2)}}{2\,m} \tag{12}$$

and the amplitude term, $A_{\rho\pi}(m,x)$, for the $\eta\pi\gamma$ final state is:

$$A_{\rho\pi}(m,x) = \frac{g^2_{\phi\rho\pi} g^2_{\rho\eta\gamma}}{24} \frac{f(m, m_{1\rho})}{|D_\rho(m_{1\rho})|^2} \tag{13}$$

while for the $\pi^0\pi^0\gamma$ a more complicated expression is given:

$$\frac{g^2_{\phi\rho\pi} g^2_{\rho\pi\gamma}}{24} \left[\left(\frac{f_1(m, m_{1\rho})}{|D_\rho(m_{1\rho})|^2} + \frac{f_1(m, m_{1\rho})}{|D_\rho(m_{2\rho})|^2} \right) + \left(\frac{f_2(m, m_{1\rho})}{|D_\rho(m_{2\rho})|^2} \right) + 2\Re e \left(\frac{f_3(m, m_{1\rho})}{D_\rho(m_{1\rho}) D_\rho(m_{2\rho})} \right) \right]. \tag{14}$$

The $g_{\phi\rho\pi}$, $g_{\rho\eta\gamma}$, $g_{\rho\pi\gamma}$ are the coupling constants while the numeric constant k is 1 (0.5) for $\eta\pi\gamma$ ($\pi^0\pi^0\gamma$) case. The variable $m_{1\rho}$ represents the invariant mass of the virtual $P\gamma$ system for a given value of m as:

$$m^2_{1\rho} = m^2_a + \frac{(m^2 + m^2_a - m^2_\pi)(m^2_\phi - m^2)}{2m^2} - \frac{(m^2_\phi - m^2)x}{m} p_{ab} \tag{15}$$

The x variable is the cosine of the γ emission angle with the respect of the ab system, thus explaining the integration between -1 and $+1$ in equation (11). In the $\pi^0\pi^0\gamma$ case, since there are identical pions π^0_1, π^0_2 in the final state, there is another possibility for the virtual $\pi^0\gamma$ system due to the π^0_1-π^0_2 exchange:

$$m^2_{2\rho} = m^2_\phi + 2m^2_\pi - m^2 - m^2_{1\rho} \tag{16}$$

Hence for this channel the $d\Gamma/dm$ is composed by three pieces: the first one for $m_{1\rho}$, the second one for $m_{2\rho}$ and the third one for their interference. The functions f, f_1, f_2 and f_3 are complicated equation in m, $m_{1\rho}$ and $m_{2\rho}$. We believe that, in the formula of Ref. [6], for a typo, the variable $m_{1\rho}$ has been susbstituted with the fixed ρ mass, m_ρ, in the corresponding propagators terms. By replacing m_ρ with $m_{1\rho}$, as done in Eq. (14), we find a $\mathrm{BR}_{\rho\pi}$ of $1.8 \cdot 10^{-5}$ in agreement with the number quoted in the cited reference and a mass spectrum as shown by the solid line in Fig. 4. If instead we use the explicit formula of Ref. [6] we found $\mathrm{BR}_{\rho\pi} = 3.8 \cdot 10^{-5}$ and a $d\mathrm{BR}/dm$ which follows the dashed line in Fig. 4. To check if we were doing everything right, we compared (see green points in Fig. 4) to an independent VMD calculation done by Rafel Escribano [13]; a good agreement is found.

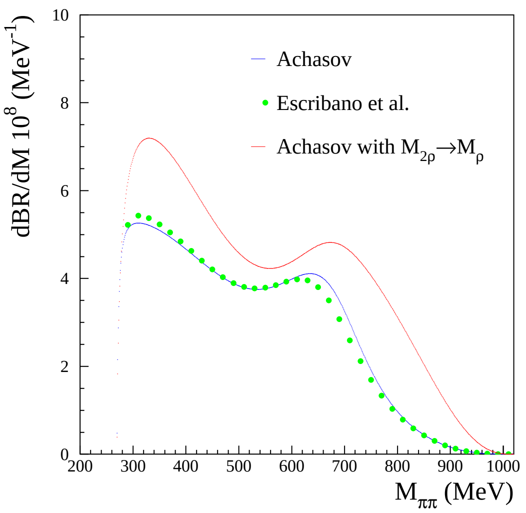

Figure 4: Comparison of dBR$/dm$ for the VMD contribution for: Eq. 14 in the text (solid), R.Escribano calculation (green points), formula from Ref. [6] (dashed).

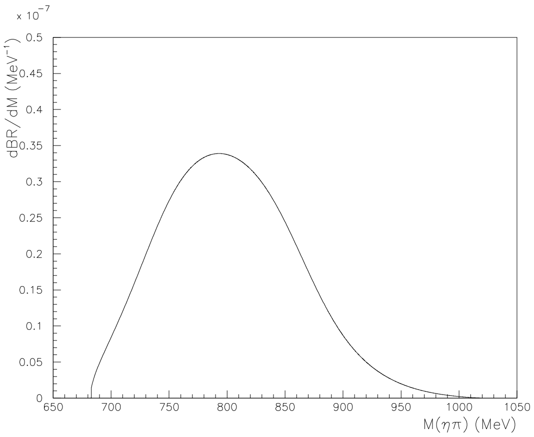

Figure 5: Expected spectrum from the $\rho\pi$ contribution to the $\eta\pi^0\gamma$ final state. The curve is normalized in such a way to give a BR of $0.5{\times}10^{-5}$.

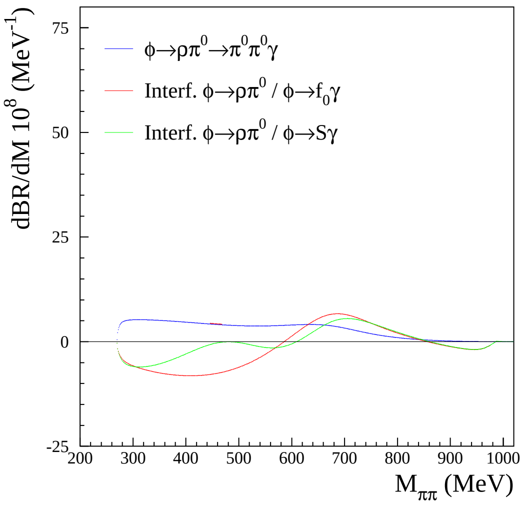

Figure 6: VMD contributions in $\phi \to \pi^0\pi^0\gamma$: VMD term (blue), interference patterns with $f_0\gamma$ (red) and with $(f_0 + \sigma)\gamma$ (green).

2.3 Interference between $S\gamma$ and VMD terms

The interference term between the scalar and VMD processes has also been considered using the explicit expression of $d\Gamma_{\rm int}/dm$ of Ref. [6].

A numerical calculation is shown in Figs. 6, 7 for the $\pi^0\pi^0\gamma$ and $\eta\pi\gamma$ final states. In the first case also the rescattering in the final state is considered introducing a $e^{i\delta_b}$ phase. The parametrization followed for $\delta_b(m)$ is $b\sqrt{m^2 - 4m_\pi^2}$, with $b = 75°/\mathrm{GeV}$, as obtained by fitting the m dependence of δ_0^0 in $\pi\pi$ elastic scattering.

2.4 Dependence of $d\Gamma/dm$ on used parameters

In order to summarize what has been said up to now, we recall that this theoretical framework is characterized by the following parameters:

1. the scalar masses m_{f_0}, m_{a_0} and m_σ;
2. the coupling $g_{\phi K\overline{K}}$ of the ϕ to $K\overline{K}$;

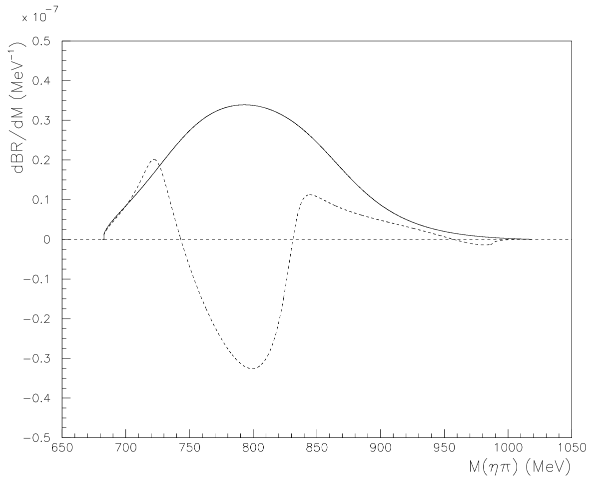

Figure 7: Expected shape of the interference contribution between $\rho\pi$ and $a_0\gamma$ to the $\eta\pi^0\gamma$ final state (dashed line) compared to the $\rho\pi$ contribution only (solid).

3. the couplings g_{Sab} of each scalar to each possible final state (in particular $ab = K\overline{K}$ and $ab = \pi\pi$ or $\eta\pi$ and the point-like coupling of the σ $g_{\phi\sigma\gamma}$);

4. the couplings $g_{\phi\rho\pi}$ of the ϕ to $\rho^0\pi^0$ and the couplings $g_{\rho\pi^0\gamma}$ and $g_{\rho\eta\gamma}$ of the ρ meson to the radiative final state.

As shown in Par. 2, some of these parameters (such as the ϕ couplings) are easily evaluated using the PDG values [14]; similarly most of the masses can also be found with high precision. On the other hand, both the couplings of the scalar particles and of the ρ^0 are known with large uncertainties and they have to be considered as free parameters.

We want to stress that the values of g_{Sab} are the relevant variables, since they allow, in principle, to discriminate between the models (see for instance [4] or [15]). In this analysis we measure directly only $g_{f_0\pi\pi}$ and $g_{a_0\eta\pi}$ while the $g_{SK\overline{K}}$ couplings are determined through the introduction of the $K\overline{K}$ loop and of D_S. By doing this the shape of $d\Gamma/dm$ depends drastically on both couplings. To explain this dependence, in Fig. 8 the mass spectrum for the $\pi^0\pi^0$ case is shown for two sets of parameters: fixing R to 4.0 and varying $g_{f_0K\overline{K}}$ (top) and fixing $g^2_{f_0K\overline{K}}/4\pi$ to 2.7 GeV^2 while varying R (bottom). The same is done in Fig. 9 for $\eta\pi^0\gamma$.

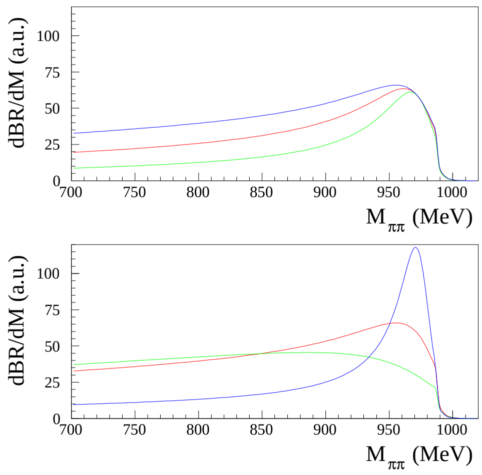

Figure 8: Dependence of $d\mathrm{BR}/dm$ on f_0 coupling constants: (top figure) R fixed to 4 with $g^2_{f_0 K\overline{K}}/4\pi$ set to 5.4 GeV^2 (green), 2.7 GeV^2 (red) and 1.3 GeV^2 (blue); (bottom figure) $g^2_{f_0 K\overline{K}}/4\pi$ fixed to 2.7 GeV^2 with R set to 8 (green), 4 (red) and 2 (blue).

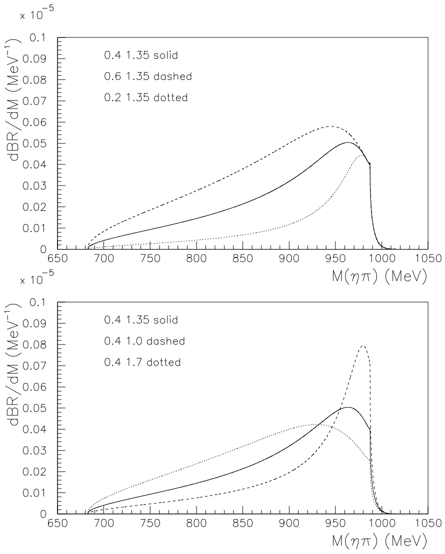

Figure 9: Dependence of $d\mathrm{BR}/dm$ on a_0 coupling constants: (top figure) $g_{a_0\eta\pi}/g_{a_0 K\overline{K}}$ fixed to 1.35 and $g^2_{a_0 K\overline{K}}/4\pi$ set to 0.2, 0.4 and 0.6 GeV^2; (bottom figure) $g^2_{a_0 K\overline{K}}/4\pi$ fixed to 0.4 GeV^2 with $g_{a_0\eta\pi}/g_{a_0 K\overline{K}}$ set to 1.0, 1.35 and 1.7.

3 Fit method

Two fits have been done: one for the $\pi^0\pi^0\gamma$ spectrum and another combined fit for the two $\eta\pi^0\gamma$ spectra. In both cases, the effect of the efficiency and of the finite resolution of the analysis method has been taken into account. The fits have been done using MINUIT. We describe separately the two fits.

3.1 Fit to the $\phi \to \pi^0\pi^0\gamma$ spectrum

To fit the raw spectrum, we have folded the theoretical function with experimental effects such as efficiency, resolution and wrong photon pairing and then minimized the χ^2 defined as:

$$\chi^2 = \sum_{i=1}^{N} \frac{(N^i_{\rm exp} - N^i_{\rm the})^2}{\sigma_i^2} \qquad (17)$$

where $N^i_{\rm exp}$ is the content of the reconstructed mass bin ($M^i_{\pi\pi}$) after subtracting the expected background ($B^i_{\rm exp}$); the binning width used is 20 MeV. $N^i_{\rm the}$ is the expected number of events in the given mass bin and is obtained by folding the theoretical function, $f(m) = d{\rm BR}/dm$, with the discrete convolution function G, and the analysis efficiency, $\epsilon_{\pi\pi\gamma}$, as follows:

$$N^i_{\rm the} = \sigma(\phi) \cdot L_{\rm int} \cdot \textstyle\sum_j \left[\, f(m_j)\Delta m \cdot {\rm G}(m_j, M^i_{\pi\pi}) \cdot \epsilon_{\pi\pi\gamma}(m_j)\right], \qquad (18)$$

where we integrated over the whole mass spectrum in bin widths, j, of 5 MeV. The convolution function ${\rm G}(m_j, M^i_{\pi\pi})$ express the probability for an event with theoretical mass, m_j, to migrate in a reconstructed mass bin i, $M^i_{\pi\pi}$. This function is composed by a gaussian smearing and a matrix of wrong photon assignment. The mass resolution is described by a gaussian with a width, σ_M, of 6 MeV while the probability of bad photon pairing, $\epsilon_{\rm wp}$, is 11% in the simulation. By fitting the $\chi^2_{\rm sel}$ distribution in the data a correction factor $\epsilon_{\rm wp}({\rm data})/\epsilon_{\rm wp}({\rm MC})$ of (1.7 ± 0.2) is found. Further details on the determination of such a function can be found in Ref. [1]. The normalization factor preceeding the sum includes the integrated luminosity $L_{\rm int}$ [16] and the ϕ production cross section, $\sigma(\phi)$ [17]. For the errors, σ_i, we have included the statistical uncertainty due to background subtraction, $N_{\rm exp} + B_{\rm exp}$, and added in quadrature the systematic errors due to background, analysis cuts and normalization.

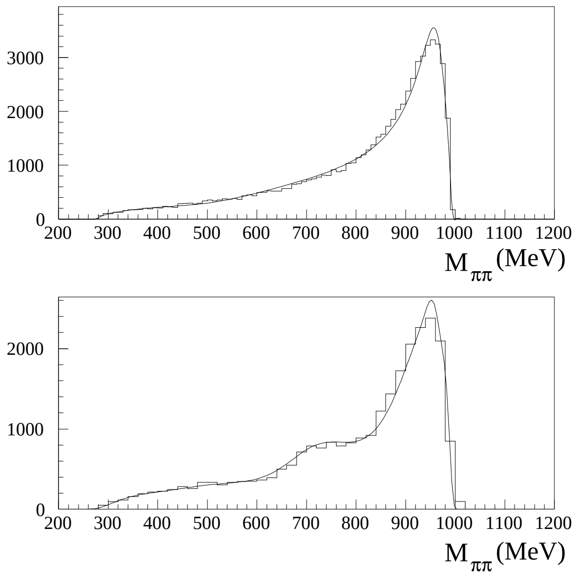

Figure 10: MC sample: generated (top) and reconstructed (bottom) $\pi^0\pi^0$ mass spectra. Both distributions are fitted with the same theoretical function before (top) and after (bottom) the folding procedure. Fit results are listed in Tab. 1.

We have first tested the reliability of the fitting method using a MC sample of $\phi \to \pi^0\pi^0\gamma$ before and after the analysis. The generated and the reconstructed mass spectra have been fitted using the theoretical function with the $(f_0 + \sigma)\gamma$ terms only before (generated spectrum) and after (reconstructed spectrum) the folding procedure (Fig. 10). The values of the extracted parameters are summarized in Tab. 1; the comparison between the parameters before and after reconstruction is excellent proving that the procedure is stable and introduces no bias on the extimation of the parameters.

Since, in the $\phi \to \pi^0\pi^0\gamma$ case, the decay can proceed trough a complicated mixture of

Table 1: MC sample: fit parameters for generated and reconstructed $\pi^0\pi^0$ mass spectrum.

	M_{f_0} (MeV)	$g^2_{f_0K\overline{K}}/4\pi$ (GeV^2)	$g^2_{f_0K\overline{K}}/g^2_{f_0\pi^+\pi^-}$
Generated	967.5 ± 0.4	1.66 ± 0.03	3.60 ± 0.04
Reconstructed	964.5 ± 1.2	1.37 ± 0.05	3.51 ± 0.14

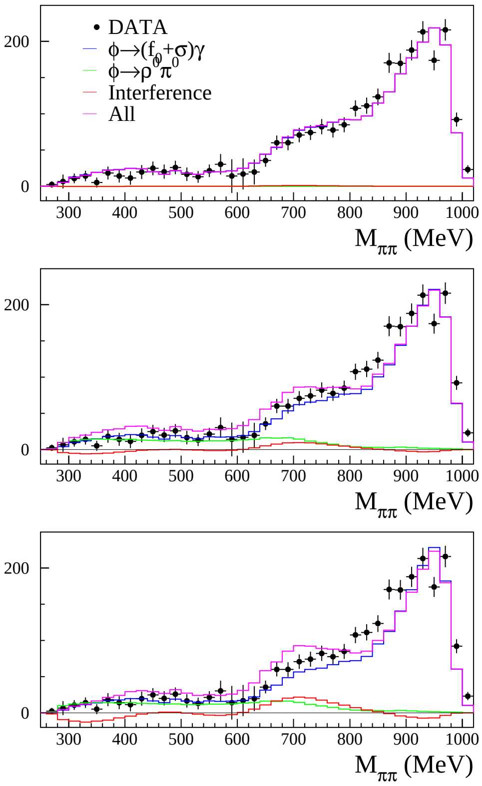

Figure 11: Fits performed to the $\phi \to \pi^0\pi^0\gamma$ data using as intermediate states $(f_0+\sigma)\gamma+\rho\pi$: (top) all parameters free, (middle) $\mathrm{BR}_{\rho\pi}$ to 1.8×10^{-5} and (bottom) $\mathrm{BR}_{\rho\pi}$ to 1.8×10^{-5} and $\cos(\phi_{VS}) = +1$.

intermediate states, we have tried to clarify the situation performing four different groups of fits over the experimental data. All the obtained parameters are reported, separately for each of this group, in Tab. 2.

- **Intermediate states: $(f_0+\sigma)\gamma+\rho\pi$**
  All the available intermediate states have been considered: the scalar term proceeding via $(f_0+\sigma)\gamma$ and the VMD term via $\rho\pi$. In Fig. 11.top the fit is performed leaving all parameters free: the M_{f_0}, the coupling constants ($g_{f_0K\overline{K}}$, $R = g^2_{f_0K\overline{K}}/g^2_{f_0\pi^+\pi^-}$, $g_{\phi\sigma\gamma}$), the VMD term normalization ($\mathrm{BR}_{\rho\pi}$) and the scalar-VMD

Fit Type	M_{f_0} (MeV)	$g^2_{f_0 K\overline{K}}/4\pi$ (GeV^2)	$g^2_{f_0 K\overline{K}}/g^2_{f_0\pi^+\pi^-}$	$g_{\phi\sigma\gamma}$	BR$_{\rho\pi}$	$\cos\phi$	χ^2/ndof
$\phi \to (f_0\gamma + \sigma\gamma + \rho^0\pi^0) \to \pi^0\pi^0\gamma$							
All free	973 ± 1	2.79 ± 0.06	4.00 ± 0.15	0.060 ± 0.004	$(2 \pm 28) \cdot 10^{-8}$	1 ± 1	43.08/31
BR$_{\rho\pi}$ fixed	968 ± 1	1.85 ± 0.03	3.71 ± 0.19	0.061 ± 0.006	—	0.43 ± 0.18	88.95/32
BR$_{\rho\pi}$ fixed $\cos\phi = +1$	966 ± 4	1.65 ± 0.24	3.73 ± 0.37	0.062 ± 0.006	—	—	97.49/33
$\phi \to (f_0\gamma + \rho^0\pi^0) \to \pi^0\pi^0\gamma$							
All free	962 ± 1	1.30 ± 0.05	3.31 ± 0.12	—	$(9 \pm 8) \cdot 10^{-7}$	1.00 ± 0.19	104.03/30
BR$_{\rho\pi}$ fixed	957 ± 5	1.03 ± 0.12	3.24 ± 0.32	—	—	0.83 ± 0.16	154.55/33
BR$_{\rho\pi}$ fixed $\cos\phi = +1$	956 ± 2	1.02 ± 0.01	3.28 ± 0.12	—	—	—	155.85/34
$\phi \to f_0\gamma \to \pi^0\pi^0\gamma$							
All spectrum	962 ± 4	1.29 ± 0.14	3.22 ± 0.29	—	—	—	109.54/34
$M_{\pi\pi} > 700$ MeV	972 ± 2	2.12 ± 0.19	3.92 ± 0.27	—	—	—	44.96/12
$\phi \to (f_0\gamma + \sigma\gamma) \to \pi^0\pi^0\gamma$							
All spectrum	973 ± 1	2.79 ± 0.12	4.00 ± 0.14	0.060 ± 0.008	—	—	43.15/33
$M_{\pi\pi} > 700$ MeV	978 ± 1	5.80 ± 7.77	4.15 ± 0.21	0.128 ± 0.065	—	—	20.51/11

Table 2: These table summarizes the fit results for the decay $\phi \to \pi^0\pi^0\gamma$: The table is organized in the four sets of fits described in the text.

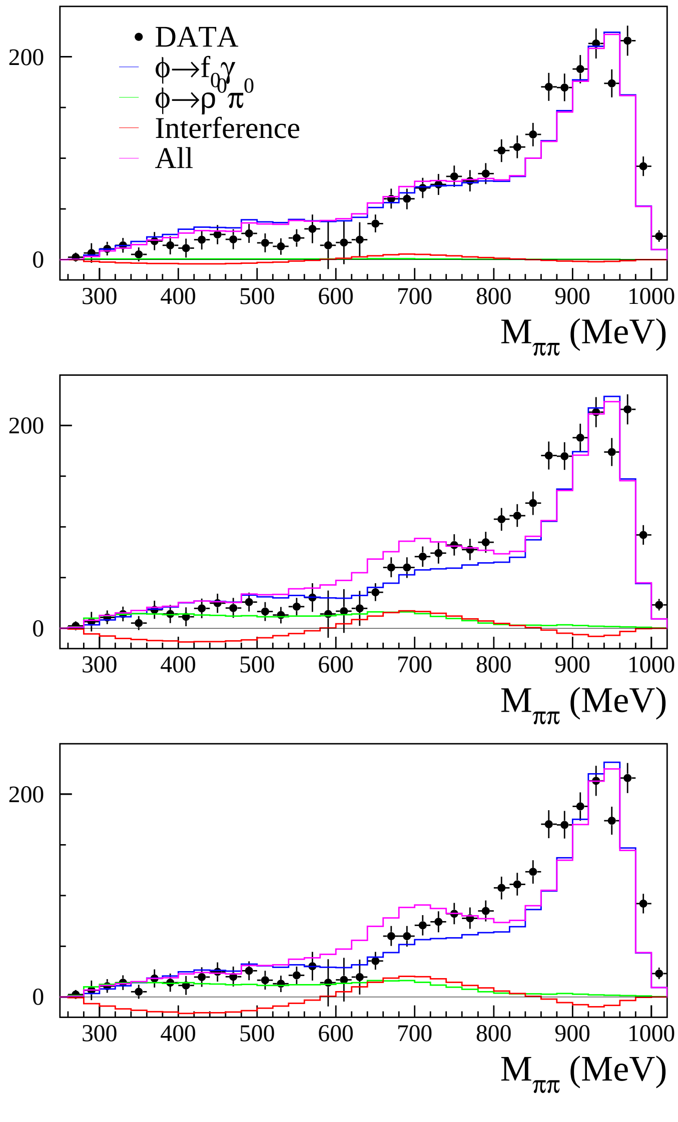

Figure 12: Fits performed to the $\phi \to \pi^0\pi^0\gamma$ data using as intermediate states $(f_0\gamma + \rho\pi)$: (top) all parameters free, (middle) $\mathrm{BR}_{\rho\pi}$ to 1.8×10^{-5} and (bottom) $\mathrm{BR}_{\rho\pi}$ to 1.8×10^{-5} and $\cos(\phi_{VS}) = +1$.

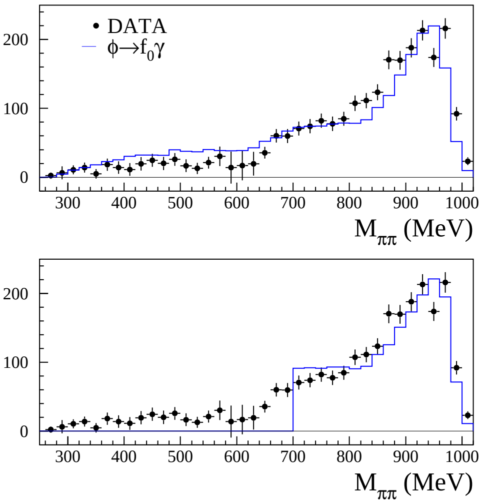

Figure 13: Fits performed to the $\phi \to \pi^0\pi^0\gamma$ data using as intermediate states $f_0\gamma$ only: (top) in the whole mass region and (bottom) $M_{\pi\pi}$ above 700 MeV.

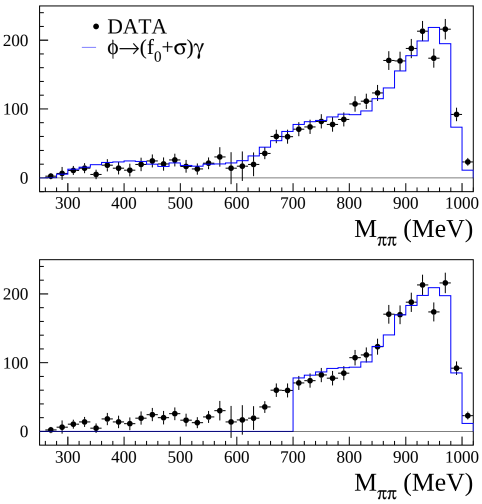

Figure 14: Fits performed to the $\phi \to \pi^0\pi^0\gamma$ data using as intermediate states $(f_0 + \sigma)\gamma$ only: (top) in the whole mass region and (bottom) $M_{\pi\pi}$ above 700 MeV.

interference phase (ϕ_{VS}). In Fig. 11.middle the same fit is performed fixing the $\mathrm{BR}_{\rho\pi}$ to 1.8×10^{-5} while still retaining ϕ_{VS} as a free parameter. Finally, in Fig. 11.bottom the fully constructive interference is used fixing $\cos(\phi_{VS})$ to +1. The negative interference has also been tested resulting in a worst χ^2. These fits shows that the $\rho\pi$ contribution is either negligible or disfavoured by the experimental shape.

- **Intermediate states: $f_0\gamma + \rho\pi$**
  In this second group, we have disregarded the possibility of a $\sigma\gamma$ contribution; the missing parameter is therefore $g_{\phi\sigma\gamma}$. Similarly to the first group, the fit performed in Fig. 12.top represents all parameters free while the fits in Figs. 12.middle-bottom use a fixed $\mathrm{BR}_{\rho\pi}$ with either a free $\cos(\phi_{VS})$ or a fully constructive interference. The data-fit agreement is really poor since the χ^2/ndf goes from 3.3 to 5.

- **Intermediate state: $f_0\gamma$ only**
  This is the simplest possible case since assumes only the $f_0\gamma$ contributing to the final state. In this case there are 3 free parameters: the M_{f_0} and the constants $g_{f_0K\overline{K}}$, R. In Fig. 13.top(bottom) the fit is performed over the whole mass range (only for masses above 700 MeV). The second fit should follow better the data than the first one since a possible VMD+$\sigma\gamma$ term should be reduced in the high $M_{\pi\pi}$ region. Still, the agreement of the theory with the data is really poor.

- **Intermediate states: $(f_0 + \sigma)\gamma$**
  In this case we consider the two contributions for $S\gamma$: the one due to f_0 via charged kaon-loops and the point-like σ. In Fig. 14.top(bottom) the fit is performed over the whole mass range (only for masses above 700 MeV). The quality of the fit is good on both cases. The value of $g_{f_0K\overline{K}}$ is not a directly measured parameter but it is obtained trough the dependence of the mass shape on the $K\overline{K}$ loop and the $K\overline{K}$ width in the D_S propagator. This parameter is therefore strongly correlated to both R and $g_{\phi\sigma\gamma}$ and the fit is unable to determine it, with small errors, whenever restricting the fit above 700 MeV.

We now try to interpret and summarize these results:

1. It is evident from the χ^2 of the fits that, independently on introducing or not the σ meson, the experimental points tend to eliminate the VMD contributions. This can be considered ackward, theoretically speaking, but we have to take into account that the coupling constants are known with a 15% error and that we cannot exclude some cancellations due to higher orders in VMD or other not considered interference schemes. In Ref. [1] we have also pointed out that, once the $S\gamma$ simulation follows the "observed" mass spectrum, the data-MC agreement in the angular distributions do not leave space to a sizeable ($\sim 20\%$) $\rho\pi$ contribution.

2. Considering the $f_0\gamma$ as the only mechanism of the decay $\phi \to \pi^0\pi^0\gamma$ is not enough. This is proven by the bad χ^2 values of the fits in the whole mass range and also with $M_{\pi\pi} > 700$ MeV.

3. A mechanism of negative interference is needed, in the region below 700 MeV, to explain the observed experimental drop of the cross-section. A similar situation is also reported from SND experiment [18], where to interpret the data a semi-empirical form of $f_0\gamma + \rho\pi$ interference is used. [4] We find much more interesting (and reasonable due to the direct measurement of E791) to consider also the contribution due to the σ meson following Ref. [9].

In Fig. 15 the spectrum after unfolding is shown with the best fit performed using $(f_0 + \sigma)\gamma$. We have also evaluated the BR contribution of each single term:

1. $\mathrm{BR}(\phi \to f_0\gamma \to \pi^0\pi^0\gamma) = (1.49 \pm 0.07) \cdot 10^{-5}$

2. $\mathrm{BR}(\phi \to \sigma\gamma \to \pi^0\pi^0\gamma) = (0.28 \pm 0.04) \cdot 10^{-5}$

A discussion on the values found for the f_0 coupling constants is reported in Par. 4 together with a comparison to other recent experiments. A test on the $K\overline{K}$ loop model consists in neglecting the width contribution of the $\eta\eta$ final state ($\Pi_S^{\eta\eta}$) in the D_S; the effect is to scale of 0.84 the value of $g^2_{f_0K\overline{K}}$ (Fig. 16).

An open item, both in the collaboration and whenever reporting to the outside world, is the width of this meson. Using the width of the $K\overline{K}$ loop model, $-\Im m(D_S(m_S)/m_S)$,

[4] The SND collaboration considers the amplitudes $S_{S\gamma}$ and $S_{\rho\pi}$ due to $\phi \to S\gamma$ and VMD respectively. The overall mass spectrum is taken as $|S_{S\gamma}|^2 + |S_{\rho\pi}|^2 + 2\cos\theta\,|S_{S\gamma}|\,|S_{\rho\pi}|$. This is true only if the two terms are real.

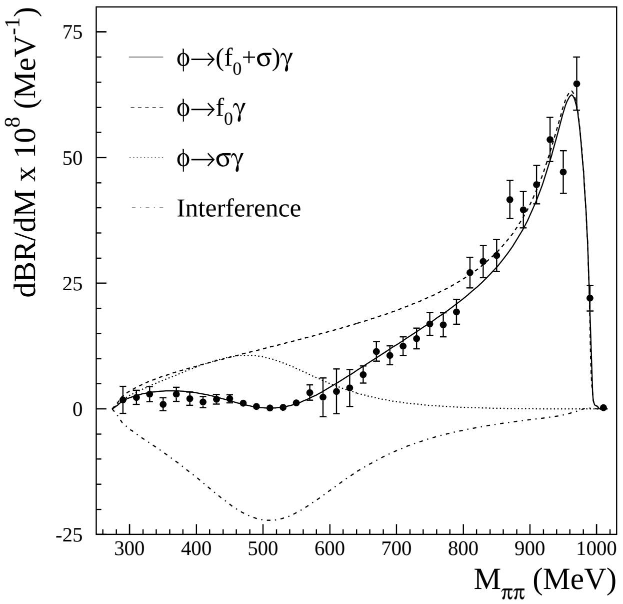

Figure 15: Unfolded $d\mathrm{BR}/dm$ spectrum for $\phi \to \pi^0\pi^0\gamma$.

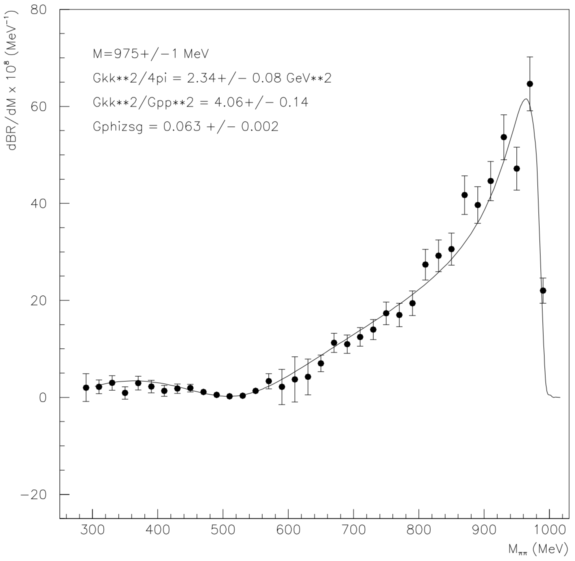

Figure 16: Fit to the $M_{\pi\pi}$ spectrum neglecting the $\Pi_{f_0}{}^{\eta\eta}$ term in the inverse propagator.

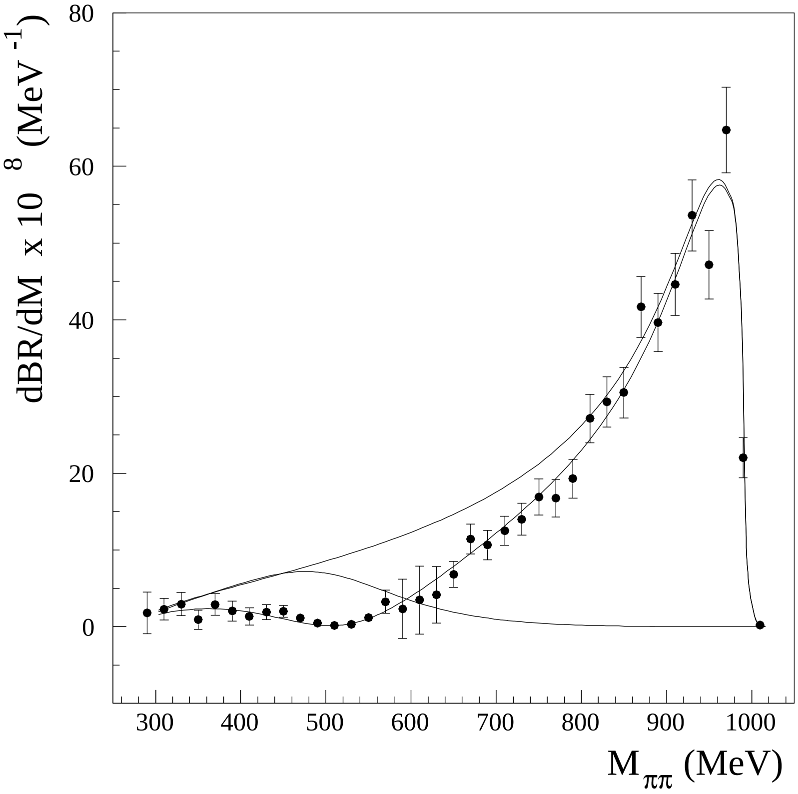

Figure 17: Fit to the $M_{\pi\pi}$ spectrum using a simple Breit-Wigner for the f_0 meson.

we find: $\Gamma_{f_0} = 257^{+40}_{-20}$ MeV. If we instead replace, in the fit procedure, the D_S with a simple BW (Fig. 17), we obtain an effective width of 113 ± 6 MeV and the coupling constants: $g^2_{f_0 K\overline{K}}/4\pi = 1.65 \pm 0.3\mathrm{GeV}^2$, $R = 5.57 \pm 1.9$, $g_{\phi\sigma\gamma} = 0.076 \pm 0.008$.

A final warning is on the determined value of $g_{\phi\sigma\gamma}$. In our fit, to simplify the formulas, we have used the same $\Gamma(f_0 \rightarrow \pi^0\pi^0)$ for both f_0 and σ mesons. Using this trick, we have incorporated in $g_{\phi\sigma\gamma}$ also the coupling difference between the two mesons to the final state. If we want to compare the values with the ones reported in [9], we have to use the correct width (324 MeV) for the σ. Using our best fit results we obtain at $M_{\pi\pi} = M_\sigma$ a value of $\Gamma(f_0 \rightarrow \pi^0\pi^0) = 453$ MeV. This means that we have overestimated the σ width of a factor $453/324 = 1.4$ and therefore, in order to mantain the same value of the cross section, $g_{\phi\sigma\gamma}$ has to be scaled up of $\sqrt{1.4} = 1.18$. Hence to compare with previous published numbers, we quote $g_{\phi\sigma\gamma} = 0.071 \pm 0.009$.

3.2 Fit to the $\phi \to \eta\pi^0\gamma$ spectrum

A combined fit has been done of the two spectra, fixing the ratio BR($\eta \to \gamma\gamma$)/BR($\eta \to \pi^+\pi^-\pi^0$) to 1.70 according to PDG. The χ^2 function has been built as follows:

$$\chi^2 = \sum_{i=1}^{N} \frac{(N^i_{\rm exp} - N^i_{\rm the})^2}{\sigma_i^2} \tag{19}$$

$N^i_{\rm exp}$ is the content of the bin i and the sum is done on the bin of both spectra; $N^i_{\rm the}$ is

$$N^i_{\rm the} = L_{\rm int}\, \sigma(\phi)\, {\rm BR}(\eta \to X) \times \sum_{j=1}^{N} M(i,j) I(j) \tag{20}$$

where $I(j)$ is the integral

$$I(j) = \int_{\rm inf_j}^{\rm sup_j} f(m; p1, p2, p3)\, dm \tag{21}$$

and where the sum is done on all the bins of each spectrum; $M(i,j)$ is a smearing matrix obtained by applying the selection procedure to Montecarlo events and evaluating the probability that an event generated in the mass bin j, is selected and reconstructed in the bin i. This matrix includes the effect of efficiency, resolution and wrong pairing between the particles of the event. It has been evaluated for both spectra (the one fully neutral and the one with charged tracks). In both cases it is mostly diagonal, with a tail of the order of 10%. The factor preceeding the sum includes the integrated luminosity $L_{\rm int}$, the ϕ production cross section and the η branching ratio in the X channel.

The function $f(m; p1, p2, p3)$ is the theoretical function, m is the variable and $p1, p2, p3$ are the 3 free parameters. The function is integrated on each bin between ${\rm inf}_j$ and ${\rm sup}_j$ that define the mass interval of each bin.

$$f(m; p1, p2, p3) = \frac{d\Gamma_{a_0}}{dm} + \frac{d\Gamma_{VMD}}{dm} \pm \frac{d\Gamma_{\rm int}}{dm} \tag{22}$$

The free parameters are:

1. the coupling $g^2_{a_0 K\overline{K}}$;
2. the ratio of couplings $g_{a_0\eta\pi}/g_{a_0 K\overline{K}}$;
3. an overall parameter for the VMD component related to the overall BR by integrating the resulting contribution.

The a_0 mass has been fixed at the PDG average 984.2 MeV and the coupling constant to $\eta'\pi$ has been also fixed (see eq.7, it is anyhow absolutely unrelevant).

The uncertainty on the i-th bin, σ_i^2, includes the statistics of data $N^i_{\rm exp}$, the background subtraction $N^i_{\rm bck}$ (relevant only in the case of fully neutral spectrum) and the statistics of the Montecarlo (N_j^{MC} is the number of MC events generated in the bin j) used to evaluate the matrix $M(i,j)$. The expression is

$$\sigma_i^2 = N^i_{\rm exp} + N^i_{\rm bck} + \sum_{j=1}^{N} \frac{M(i,j)(1-M(i,j))}{N_j^{MC}}\, I(j)^2 \tag{23}$$

where a binomial fluctuations has been assumed for the values of $M(i,j)$ and $I(j)$ is the integral defined above (see Eqs. (20) and (21)). Fig. 18 shows the result of the combined fit obtained without interference. The first two plots show the comparison between data and fit for the two samples while in the third plot the theoretical curve for the a_0 contribution is shown.

The fit has been tried adding and subtracting the interference term and also without the interference term. Moreoever the fit has been also tried separately for the two spectra. The results are reported in Tab. 3. It can be noticed that in some cases, the fit converges to the lower limit of $BR(VMD)$. In this case the MINUIT result for the estimation of parameter error and covariance matrix are not completely reliable, so they have been omitted. Apart from this, the fits show all a good agreement in the parameter values.

The value of $BR(\phi \to a_0\gamma)$ is evaluated by integrating the part of the theoretical function corresponding to the a_0 contribution. Such an integral is clearly a function of the parameters of the fit, so that in order to have a reliable estimate of its uncertainty the parameter error matrix has to be taken into account toghether with the derivatives of $BR(\phi \to a_0\gamma)$ respect to the relevant parameters. The parameter error matrix is taken from the MINOS output of MINUIT while the derivatives are evaluated numerically. The result for the combined noint. fit is:

$$BR(\phi \to a_0\gamma) = (7.36 \pm 0.71) \times 10^{-5} \tag{24}$$

In order to test the reliability of the fit method, a Montecarlo sample has been generated with a distribution given by the function $f(m)$ with known parameters (those obtained by the fit have been used) and with no interference. The sample dimension is

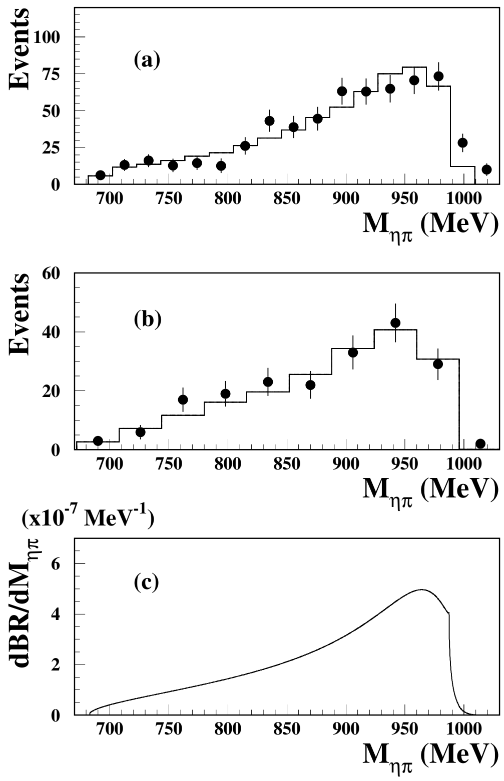

Figure 18: Result of the combined fit: comparison of data vs. fit for (a) the neutral sample and (b) the charged sample. In (c) the theoretical curve for the a_0 contribution is shown.

Table 3: Results of the fits: comb. is combined fit, neut. and char. are the fit with only one of the two spectra. When BR(VMD) goes to 0 (at limit according to MINUIT) the fit is unstable and the errors on the parameters are not reliable.

Fit type	$g^2_{a_0K\overline{K}}/4\pi$ (GeV^2)	$g_{a_0\eta\pi}/g_{a_0K\overline{K}}$	BR(VMD)$\times 10^{-5}$	χ^2/ndof	BR($\phi \to a_0\gamma$) $\times 10^{-5}$
comb. noint	0.401$\pm$ 0.036	1.350$\pm$0.090	0.49$\pm$0.54	26.8/24	7.36
comb. +int	0.391$\pm$ 0.042	1.341$\pm$0.092	0.76$\pm$0.79	26.6/24	7.14
comb. $-$int	0.428	1.381	0	27.5/24	7.81
neut. noint	0.418	1.360	0	20.8/14	7.73
neut. +int	0.395$\pm$ 0.033	1.332$\pm$0.079	0.70$\pm$0.67	18.7/14	7.17
neut. $-$int	0.418	1.360	0	20.8/14	7.73
char. noint	0.369$\pm$ 0.055	1.34$\pm$0.15	1.3$\pm$0.8	4.4/7	6.70
char. +int	0.414	1.427	0	6.4/7	8.06
char. $-$int	0.383$\pm$ 0.059	1.35$\pm$0.17	0.98$\pm$0.73	3.4/7	7.00

approximately a factor 7 larger than the data for both spectra. On this sample the same fits have been applied. In Tab. 4 the results are compared with the "true" values. A significant deviation respect to the "true" value is observed for $g^2_{a_0K\overline{K}}/4\pi$ that turns to be systematically lower by about 0.05 respect to the "true" value. This systematic effect is of the same level of the statistical uncertainty of the data so it has to be considered. We can either correct the result or use the systematic effect found as an estimate of a systematic uncertaitny. The two possibilities correct the result shown in the first line of Tab. 3 as:

$$g^2_{a_0K\overline{K}}/4\pi = (0.45 \pm 0.04 \pm 0.01)\ \mathrm{GeV}^2 \tag{25}$$

$$g^2_{a_0K\overline{K}}/4\pi = (0.40 \pm 0.04 \pm 0.05)\ \mathrm{GeV}^2 \tag{26}$$

Fig. 19 shows the fitting function $f(m)$ compared to the unfolded data expressed as $d\mathrm{BR}/dM$. Unfolding has been done for each spectrum according to the

$$(d\mathrm{BR}/dM)^j = \sum_{i=1}^{N} U^{-1}(i,j) N^i_{exp} \tag{27}$$

where the matrix $U^{-1}(i,j)$ is obtained inverting the matrix $U(i,j) = M(i,j) \times L_{int}\sigma(\phi)\mathrm{BR}(\eta \to X)$ for both final states X. The result of this unfolding procedure are reported in Tab. 5. Uncertainties are evaluated neglecting the contribution of M^{-1}.

Table 4: $\phi \to \eta\pi^0\gamma$ simulated events: comparison of the fit results with the "true" MC values.

Fit type	$g^2_{a_0 K\overline{K}}/4\pi$ (GeV^2)	$g_{a_0\eta\pi}/g_{a_0 K\overline{K}}$	BR(VMD)$\times 10^{-5}$	χ^2/ndof
"true" values	0.401	1.35	0.52	
comb. noint	0.348$\pm$ 0.010	1.403 $\pm$ 0.029	0.77$\pm$ 0.18	33.6/24
	(-0.052$\pm$0.010)	(0.053$\pm$0.029)	(0.15$\pm$0.18)	
neut. noint	0.343$\pm$ 0.007	1.413 $\pm$ 0.035	0.53$\pm$ 0.19	4.6/14
	(-0.058$\pm$0.007)	(0.063$\pm$0.035)	(0.01$\pm$0.19)	
char. noint	0.376$\pm$ 0.032	1.368 $\pm$ 0.085	1.16$\pm$ 0.39	7.1/7
	(-0.024$\pm$0.032)	(0.018$\pm$0.085)	(0.64$\pm$0.39)	

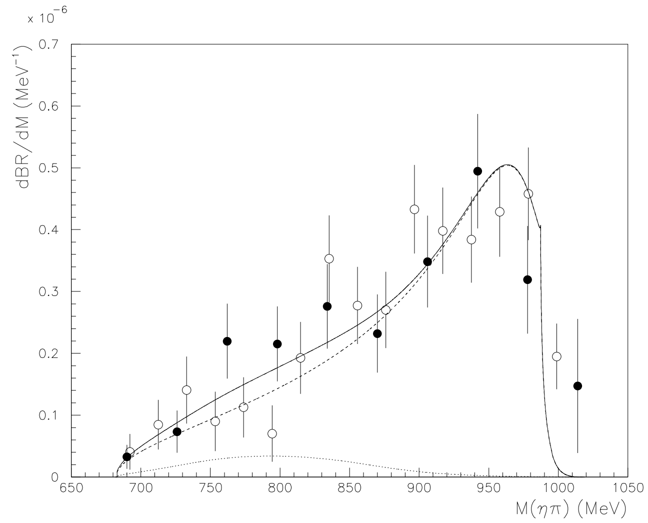

Figure 19: Comparison of unfolded distribution with the theoretical function found. The contribution from $\rho\pi$ and a_0 are also shown.

Table 5: Table of unfolded values of $(d\mathrm{BR}/dM)$ as a function of M for $\eta \to \pi^+\pi^-\pi^0$ sample (upper part of the table) and $\eta \to \gamma\gamma$ sample (lower). The values of $M(\eta\pi^0)$ are taken at the centre of each bin.

$M(\eta\pi^0)$ (MeV)	$(d\mathrm{BR}/dM) \times 10^{-7} MeV^{-1}$	uncertainty
690.	0.33	0.19
726.	0.73	0.34
762.	2.20	0.61
798.	2.15	0.61
834.	2.76	0.68
870.	2.32	0.63
906.	3.48	0.74
942.	4.94	0.93
978.	3.19	0.87
1014.	1.47	1.08
692.	0.41	0.29
712.	0.84	0.40
733.	1.41	0.54
753.	0.90	0.48
774.	1.13	0.49
794.	0.70	0.46
815.	1.93	0.58
835.	3.53	0.70
856.	2.77	0.62
876.	2.70	0.62
897.	4.33	0.72
917.	3.98	0.70
937.	3.84	0.70
958.	4.29	0.73
978.	4.58	0.75
999.	1.95	0.53
1019.	0.66	0.22

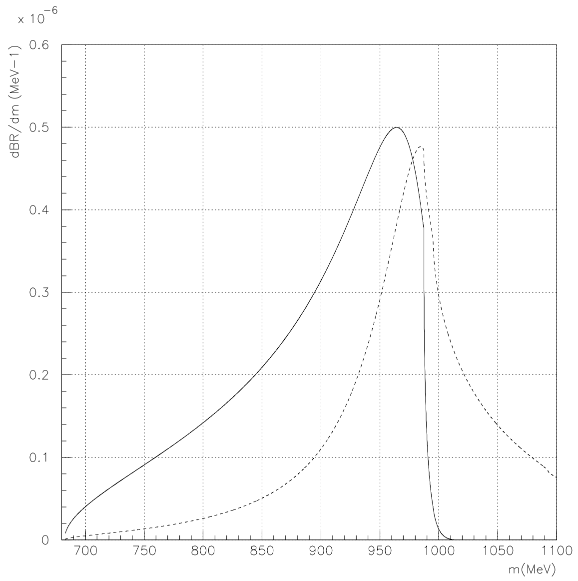

Figure 20: Shape of the a_0 spectrum before (solid) and after (dashed) removal of the $\phi \to a_0\gamma$ distortion. The Breit-Wigner width of the dashed curve is around 70 MeV.

The shape found and shown in Fig. 18.c, is strongly affected by the $\phi \to a_0\gamma$ decay mechanism and cannot be simply compared to the the a_0 shape observed by several experiments that looks at the inclusive $\eta\pi^0$ mass spectra produced in fixed target od $p\overline{p}$ collisions. In order to make this comparison the quantity

$$\frac{d\Gamma(\phi \to a_0\gamma \to \eta\pi^0\gamma)/dm}{\Gamma(\phi \to a_0\gamma)} = \frac{2m^2}{\pi}\frac{\Gamma(a_0 \to \eta\pi^0\gamma)}{|D_{a_0}|^2} \tag{28}$$

is evaluated and shown in Fig. 20. It rapresents the a_0 shape after removal of the peculiar distortion due to decay $\phi \to a_0\gamma$. It exhibits a tipical Breit-Wigner shape and the width is around 70 MeV.

4 Discussion of the results

The results obtained can be compared with other existing experiments and with theoretical expectations based on different models of f_0 and a_0.

Table 6: Comparison of the results of the present analysis with existing experiments. R_{f_0}, R_{a_0} are defined as $g^2_{f_0 K\overline{K}}/g^2_{f_0\pi^+\pi^-}$, $g^2_{a_0 K\overline{K}}/g^2_{a_0\eta\pi}$ respectively.

Experiment	$g^2_{f_0 K\overline{K}}/4\pi$	$g^2_{a_0 K\overline{K}}/4\pi$	R_{f_0}	R_{a_0}
KLOE	2.79 ± 0.12	0.40 ± 0.04	4.00 ± 0.14	0.55 ± 0.07
SND	$2.47^{+0.73}_{-0.51}$	$1.4^{+9.4}_{-0.9}$	4.6 ± 0.8	1.8 ± 1.5
CMD-2	2.44 ± 0.73		6.1 ± 2.0	
WA102	$0.40 \pm 0.04 \pm 0.04$		1.6 ± 0.4	
FNAL-E791	$0.02 \pm 0.04 \pm 0.03$		0.2 ± 0.4	
BNL-E852				0.91 ± 0.10
Crystal Barrel				$0.87 \div 1.15$

4.1 Comparison with other experiments

The scalars f_0 and a_0 have been observed in several experiments with different production mechanisms. Most experiments give measurements of mass and width. Only recently some experiments have applied a fit to the mass spectrum in order to extract the relevant couplings. The most relevant are the two Novosibirsk experiments SND [18, 19] and CMD-2 [20], where the mesons are produced in an e^+e^- ϕ-factory as in KLOE, Crystal Barrel at LEAR [21, 22], WA102 [23] at CERN, E791 at Fermilab [24] and the Brookhaven experiment E856 [25]. In Tab. 6 a comparison of the results between KLOE and these experiments is shown. A reasonable agreement is found between KLOE and the two Novosibirsk experiments while significant discrepancies are found respect to fixed target experiments, where a slightly different formulation of the fit is used.

4.2 Comparison with theoretical expectations

The main motivation of the analysis presented here is to compare our data with $q\overline{q}$ and $qq\overline{qq}$ models. These two models make predictions based on SU(3) algebra assuming no OZI-violations for the ratios of the coupling constants. Qualitative predictions are available for the absolute value of the couplings. Tab. 7 shows these predictions compared with KLOE results. The predictions have been evaluated using a value of $\theta_P = -13.7°$ for the pseudoscalar mixing angle [26]. From this comparison we can notice that:

Table 7: Comparison of the results of the present analysis with predictions from $q\overline{q}$ and $qq\overline{qq}$ models. $q\overline{q}$ (a) and (b) refer to either $f_0 = (u\overline{u} + d\overline{d})/\sqrt{2}$ (a) or $f_0 = s\overline{s}$.

Experiment	$g^2_{f_0 K\overline{K}}/4\pi$	$g^2_{a_0 K\overline{K}}/4\pi$	R_{f_0}	R_{a_0}
KLOE	2.79 ± 0.12	0.40 ± 0.04	4.00 ± 0.14	0.55 ± 0.07
$qq\overline{qq}$	”superallowed”	“superallowed”	$4 \div 8$	1.2
$q\overline{q}$ (a)	“OZI-allowed”	“OZI-forbidden”	4	0.43
$q\overline{q}$ (b)	“OZI-forbidden”	“OZI-forbidden”	0.5	0.43

1. the f_0 parameters are not compatible with $q\overline{q} = u\overline{u} + d\overline{d}$ (R_{f_0} is too large and $g_{f_0 K\overline{K}}$ is also too large); on the other hand R_{f_0} is compatible both with $q\overline{q}q\overline{q}$ model parameters and with $s\overline{s}$ expectation;

2. the a_0 coupling $g_{a_0 K\overline{K}}$ is too small respect to $q\overline{q}q\overline{q}$ predictions; R_{a_0} seems to indicate better agreement with $q\overline{q}$ model.

Predictions for the value of the branching ratios have been done also in the framework of the linear sigma model[8] and in the unitarized chiral model approach [27] showing rather good agreement.

References

[1] S.Giovannella and S.Miscetti, KLOE Memo 244 05/01 and KLOE Note 178 04/02;

[2] P.Gauzzi, KLOE Memo 247 06/01;

[3] C.Bini, D.Leone, KLOE Memo 250 10/01;

[4] N.N.Achasov, V.N.Ivanchenko, Nucl.Phys. B**315**, 465 (1989);

[5] N.N.Achasov, V.V.Gubin, Phys.Rev.D**56**, 4084 (1997);

[6] N.N.Achasov, V.V.Gubin, Phys.Rev.D**63**, 094007 (2001);

[7] A.Bramon, A.Grau, G.Pancheri, LNF-92/011 (P) 02/1992;

[8] A.Bramon et al., Phys.Lett. B**494**, 221 (2000);

[9] A.Gokalp O.Yilmaz, Phys. Rev. D 64 (2001) 053017;

[10] E.M.Aitala et al., Phys. Rev. Lett. 86 (2001) 770;

[11] D.M.Asner et al., Phys. Rev. D 61, (2000);

[12] S.Fajfer, R.J.Oakes, Phys.Rev. D**42**, 2392 (1990);

[13] R.Escribano, private communication;

[14] D.Groom et al., Eur.Phys.J. C15 (2000) 1;

[15] R.L.Jaffe, Phys.Rev. D15, 267 (1977); D17, 1444 (1978);

[16] A. Denig, KLOE Phisics Workshop at la Biodola, 23th-25th May 2001 (*http://www.lnf.infn.it/kloe/private/biodola/denig.pdf*) and private communication;

[17] S.Giovannella and S.Miscetti, KLOE Note 177 04/02;

[18] M.N.Achasov et al., Phys.Lett. B485 (2000) 349-356;

[19] M.N.Achasov et al., Phys.Lett. B479 (2000) 53-58;

[20] R.R.Akhmetshin et al., Phys.Lett. B462 (1999) 380-388;

[21] C.Amsler et al., Phys.Lett.B333 (1994) 277;

[22] D.V.Bugg et al., Phys.Rev.D50 (1994) 4412;

[23] D.Barberis et al., Phys.Lett. B462 (1999) 462-470;

[24] E.M.Aitala et al., Phys.Rev.Lett. 86, 5 (2001) 765-769;

[25] S.Teige et al., Phys.Rev.D59 012001 (2001);

[26] F.Ambrosino, KLOE Memo 266 3/02;

[27] E.Marco et al., Phys.Lett. B470 (1999) 20;